High-Resolution Modeling of Size-Resolved Stratospheric Aerosol

A. S. KOZIOL AND J. PUDYKIEWICZ

Atmospheric Environment Service, Dorval, Quebec, Canada

(Manuscript received 22 July 1997, in final form 13 January 1998)

ABSTRACT

In certain applications the, so-called, bin or sectional models are not adequate to model aerosol or cloud droplets. Therefore, the authors developed a continuous, high-resolution in size model of aerosol. The application of this model to the stratospheric Junge layer is presented. The equations with which to model the aerosol as well as the physics underlying the equations are described in detail. In the authors' approach, the role of vertical advection is emphasized, and in particular, a realistic diffusion coefficient that eliminates vigorous, artificial mixing between vertical levels is used. The equations are solved using appropriate and accurate numerical methods. As a test, the one-dimensional version of the model is applied to the stratospheric aerosol for both quiescent and volcanic periods. The results are able to capture some characteristics of the Junge layer, which cannot be modeled with bin models with large diffusion. It is also found that the effect of a volcanic eruption on the aerosol population can be long lasting, up to five or six years.

1. Introduction

In the late 1950s and early 1960s, it was experimentally established that a persistent sulfate aerosol layer exists in the stratosphere (Junge et al. 1961). Each single droplet of such aerosol is composed of a liquid or blurry solution of water and sulfuric acid with, possibly, a solid core of soluble or insoluble substances inside. Junge et al. (1961) also proposed a mechanism within the stratosphere that seems to be responsible for maintaining the aerosol layer. [This was later elaborated; see, e.g., the review article by Turco et al. (1982).] According to the theory, sulfur-bearing gases of tropospheric origin, like SO_2 and OCS, constitute the major precursors of stratospheric aerosol. More recently, Crutzen (1976) estimated that during quiet periods between volcanic eruptions OCS rather than SO_2 is injected into the stratosphere, thus being the major precursor of sulfuric aerosol during such periods. On the other hand, large amounts of SO_2 injected during volcanic eruptions dominate the source of stratospheric sulfur aerosol. SO_2 undergoes oxidation through the reaction with the OH radical to produce vapor of sulfuric acid, whereas OCS through photolysis and through reaction with single oxygen is converted to SO_2, and then, ultimately to H_2SO_4. [It has been also speculated that CS_2 may play a role similar to OCS (Sze and Ko 1979).]

In the stratosphere, neither homogeneous nor heterogeneous nucleation of pure sulfuric acid is efficient enough to account for the formation of aerosol. However, heteromolecular nucleation of water and sulfuric acid vapors onto Aitken nuclei was found to be quite effective in producing aerosol (Hamill et al. 1977b). Later, after laboratory experiments (Roedel 1979; Ayers et al. 1980) and observational evidence (Sheridan et al. 1992), it was concluded that during volcanic episodes not only heterogeneous-heteromolecular but also homogeneous-heteromolecular nucleation must take place (Zhao et al. 1995). Further growth of freshly nucleated drops is assured by the combined processes of condensation and coagulation (Hamill et al. 1977a). Additional factors that affect the aerosol growth are of dynamic nature. These are vertical and horizontal mixing by small-scale turbulence, meridional hemispheric circulation, horizontal and vertical mixing by large-scale troposphere–stratosphere exchange, and gravitational sedimentation (Junge et al. 1961).

Modeling of the Junge layer, which started in the 1970s, soon became important not only because of the scientific curiosity of how the layer is produced and maintained but also because of a significant effect of the sulfur aerosol layer on both global climate modeling and heterogeneous chemistry of ozone and certain man-made chemicals persistent in the stratosphere (Hoffman 1990). Measurements of the aerosol concentration in the Junge layer show that the vertical profiles of the aerosol mixing ratios taken at different locations look remarkably similar with respect to the height of the tropopause. Thus, the first models were one-dimensional. The model developed by Turco et al. (1979) includes both Aitken nuclei and sulfate aerosol modeling as well as calcu-

Corresponding author address: Anna Koziol, Modelling and Integration Research Division, Atmospheric Environment Service, 2121 Trans-Canada Highway, Dorval, PQ, H9P 1J3 Canada.
E-mail: anna.koziol@ec.gc.ca

lations of the sulfate aerosol chemistry pertinent to the problem. Solutions of the aerosol equations were obtained using a heuristic bin method—each bin corresponding to a certain range of drop sizes; physical and chemical processes being responsible for shuffling drops between bins. This model, later modified by Toon et al. (1988), has been very successfully applied to various problems concentrated around the Junge layer, as well as other cloud and aerosol problems (e.g., Jensen et al. 1996). The Turco model or its derivatives were used to estimate the effect of heterogeneous chemistry (on aerosol surface) on ozone depletion and the effect of volcanic eruptions on radiation (Turco et al. 1983), to assess the impact of aircraft sulfur emission (Pitari et al. 1993), and to solve other problems related to the physics and chemistry of the middle atmosphere. A similar in principle bin model was developed by Tie et al. (1994), and subsequently, used to estimate global effects of major volcanic eruptions. The above-mentioned modeling effort has been very successful in capturing many characteristics of the Junge layer.

In this paper, we present a new approach to the numerical treatment of the stratospheric aerosol. We have developed a continuous, high-resolution in size model of the stratospheric aerosol. The physical and chemical properties of the aerosol included in our model are essentially similar to those present in the previously mentioned models. The significant difference consists of the numerical discretization of the equations. Our primary motivation is to better understand the evolution of the background aerosol spectra as well as those under the influence of volcanic eruptions. In particular, we aim toward a more realistic description of diffusion and small-scale advective motion. The importance of advection has often been neglected by assuming large unrealistic diffusion coefficients. Vigorous mixing introduced as a consequence of the high diffusion coefficient may in turn obscure some aspects of the change of the aerosol spectra with height. Lack of the ability of models to correctly represent certain characteristics of the background aerosol spectra as a function of height was noticed by Hoffman and Rosen (1981). We think that more accurate numerical methods may lead to a possible solution of this or similar problems. Additionally, we expect that our approach may provide us with a significant insight into some mechanisms of aerosol formation that cannot be examined experimentally because of instrumental limitations.

The version of our model described here is one-dimensional. However, the numerics were tailored to serve as an interacting module to be later used with three-dimensional dynamic models. Because of a complex, nonlinear character of the aerosol–chemical species system, we want to first verify how our model performs in a one-dimensional setting. The results are also expected to provide useful information about the behavior of the aerosol spectra.

In the following three sections, we describe in detail the physical, chemical, and dynamical processes and the system of equations with which to represent them. In section 5, we outline our numerical experiment. Then, in section 6, we present our numerical approach. Finally, we discuss our results.

2. Physical processes of sulfate aerosol

a. Variables representing aerosol

For an adequate description of the stratospheric aerosol, three types of aerosol are taken into account. These are liquid drops formed in the process of homogeneous nucleation, $n_w(V)$, liquid drops formed on nuclei, $n(V)$ (nuclei retaining their identity inside drops are called cores), and finally, solid particles: either Aitken nuclei or, in the case of a volcanic eruption, ash particles, $\hat{n}(V)$. (In figure legends we call these three types for short liquid, mixed, and solid.) Because of the necessity to keep track of cores, the distribution function, $\eta(V, U)$—the number concentration of drops of volume V with cores of volume U is introduced. The zeroth, first, second, and third moments of distribution $\eta(V, U)$ are:

$$n(V) = \int_0^V \eta(V, U)\, dU \qquad \theta(V) = \int_0^V U\eta(V, U)\, dU,$$

$$\epsilon(V) = \int_0^V U^2\eta(V, U)\, dU \quad \zeta(V) = \int_0^V U^3\eta(V, U)\, dU. \tag{1}$$

Note that the zeroth moment of $\eta(V, U)$ is equal to the total number of aerosol particles with volume V; that is, $n(V)$. The first moment $\theta(V)$ and the second moment $\epsilon(V)$ are sufficient to calculate distribution $\eta(V, U)$ if only the form of a two-parameter distribution is assumed (e.g., Gaussian, lognormal). These quantities must be modeled together with concentrations. The third moment, $\zeta(V)$, as it will be shown later, must be calculated to close equations describing condensation of water vapor. The total number of dependent variables for which to solve the continuity equation is five. Below, we describe both the physical processes and the equations that govern them.

b. Heteromolecular nucleation of water and sulfuric acid

On the basis of observations and laboratory measurements, it has been hypothesized that the stratospheric aerosol layer is formed by both homogeneous-heteromolecular and heterogeneous-heteromolecular nucleation of water and sulfuric acid vapors. This hypothesis is essentially adopted in numerical models. Here, we briefly present these elements of the nucleation theory that are relevant to our model. The details can be found in Hamill et al. (1977a) and Yue and Hamill (1979).

In the stratosphere, the concentration of water molecules is much higher than that of sulfuric acid molecules. As a consequence, many mathematical simplifications can be made, in particular, the rate of homogeneous-heteromolecular nucleation can be written:

$$\mathcal{J}^{\text{homo}} = 4\pi r^{*2}\beta_A n_W \exp(-\Delta G^*/kT), \tag{2}$$

where r^* is the critical radius (radius of a stable nucleus), k the Boltzmann constant, n_W the concentration of water molecules, T the absolute temperature, ΔG^* the critical value of the Gibbs free energy barrier, and β_A, the impinging rate of acid molecules:

$$\beta_A = n_A\left(\frac{kT}{2\pi m_A}\right)^{1/2}, \tag{3}$$

n_A and m_A being, respectively, the concentration of sulfuric acid and the mass of a single molecule of sulfuric acid. Nair and Vohra (1975) derived the following for r^* and ΔG^*:

$$r^* = \frac{2\sigma\nu^*}{RT\ \ln S^*} \qquad \Delta G^* = \frac{4}{3}\pi\sigma r^{*2}, \tag{4}$$

where

$$S^* = \left(\frac{p_A}{p_A^0}\right)^{\chi^*}\left(\frac{p_W}{p_W^0}\right)^{(1-\chi^*)}, \tag{5}$$

R is the universal gas constant; σ is the surface tension of the solution; p_A and p_A^0 are, respectively, the ambient pressure of H_2SO_4 and the equilibrium vapor pressure of H_2SO_4 vapor over a flat surface of the solution (p_W and p_W^0 are the corresponding pressures for water); $\mathcal{X}^*$ is the mole fraction of H_2SO_4 in the solution; and $\mathcal{V}^*$ is the molar volume of the solution. Here $\mathcal{X}^*$ and $\mathcal{V}^*$ can be expressed in terms of the mass ratio of the sulfuric acid in the solution, W (W is also defined at the equilibrium point but the asterisk is omitted for clarity). In particular,

$$\chi^* = \frac{WM_W}{WM_W + (1 - W)M_A},$$

$$\nu^* = \frac{1}{\rho}\frac{M_A M_W}{WM_W + (1 - W)M_A}, \tag{6}$$

$$W = \frac{N_A M_A}{N_A M_A + N_W M_W}, \tag{7}$$

where M_A and M_W are the molecular weights of, respectively, H_2SO_4 and H_2O, and ρ is the density of the solution. The approximate expression for W as a function of temperature and water vapor pressure was derived by Steele and Hamill (1981), and after Hoffman and Oltmans (1992), W can be written:

$$W = 1 - \left[18.66\exp\left(-\frac{T}{50.8}\right) + 0.1239(T - 180)^{-1.37}p_W\right]. \tag{8}$$

The remaining physical parameters necessary to calculate the nucleation rate, p_W^0, p_A^0, and σ, are taken, respectively, from Gmitro and Vermeulen (1964), Ayers et al. (1980), and Sabinina and Terpugov (1935).

The heterogeneous-heteromolecular nucleation of an aqueous solution of sulfuric acid may occur onto soluble particles, ions, flat insoluble surfaces (large particles—radii greater than 0.05 μm can be counted into this category), and insoluble particles (Hamill et al. 1977a). Only two latter cases are considered here. This is because the rate of nucleation onto soluble particles cannot be determined without the knowledge of equilibrium pressures of a three-component system that have not been measured. The nucleation rates onto ions are known but are very low in comparison with those onto insoluble surfaces and particles (Hamill et al. 1977a).

Let us now consider nucleation onto insoluble particles. Fletcher (1958) derived an expression for the Gibbs free energy difference for the case of heterogeneous-homomolecular nucleation on spherical particles. Hamill et al. (1977a) extended these ideas and obtained the nucleation rate for the case of heterogeneous-heteromolecular nucleation as follows:

$$\mathcal{J}^{\text{hetero}} = 4\pi r^{*2}\beta_A\hat{n}\exp(-\Delta G^*/kT) = \mathcal{N}^{\text{hetero}}\hat{n}, \tag{9}$$

where $\mathcal{J}^{\text{hetero}}$ is the rate of nucleation on particles of concentration $\hat{n}$. For simplification and because of the lack of reliable information, the above equation was derived with the assumption that all stratospheric particles have perfectly wettable surfaces.

c. Condensation and evaporation of sulfuric acid

Activated small aerosol droplets grow by binary condensation of H_2SO_4 and H_2O. Drops are generally in equilibrium with the surrounding water vapor, but high supersaturations with respect to sulfuric acid are common. Still, the aerosol growth is largely controlled by the ambient concentration of water vapor. This is because the number of collisions with water molecules per unit time encountered by a growing drop is 10 million times larger than that with sulfuric acid molecules. Therefore, water vapor partial pressure as well as ambient temperature control the equilibrium mass fraction of sulfuric acid (Steele and Hamill 1981). For a given temperature and water vapor partial pressure, the sequence of events is as follows. First, drops grow by catching occasional H_2SO_4 molecules. This, in turn, upsets the equilibrium with water vapor. Water vapor molecules are then instantaneously condensed onto drops so the equilibrium state is maintained, and so on.

Let us estimate the growth rate of the drop radius due to condensation of sulfuric acid as follows:

$$\frac{dr}{dt} = \frac{dr}{dN_A}\frac{dN_A}{dt} = \frac{dr}{dN_A}\phi_A, \tag{10}$$

where ϕ_A is the flux of sulfuric acid molecules onto the drop. Fuchs and Sutugin (1971) derived an expression for ϕ_A, which is valid for both small and large Knudsen numbers:

$$\phi_A = \frac{4\pi r D n_A}{1 + \lambda \mathrm{Kn}}, \tag{11}$$

where n_A is the ambient concentration of sulfuric acid molecules, Kn is the Knudsen number, D is the diffusion coefficient, and the parameter λ is defined as:

$$\lambda = \frac{1.333 + 0.71\mathrm{Kn}^{-1}}{1 + \mathrm{Kn}^{-1}} + \frac{4(1 - \alpha)}{3\alpha}. \tag{12}$$

Here α, the so-called sticking coefficient, is assumed to be equal to unity because there is no reliable information to assume otherwise. The diffusion coefficient was calculated by Fuchs and Sutugin (1971):

$$D = \frac{1}{3}\left(\frac{8kT}{\pi m_A}\right)^{1/2} l_{\mathrm{eff}}, \tag{13}$$

where m_A is the mass of a single sulfuric acid molecule, and the ''effective'' mean free path of sulfuric acid molecules in air, l_{eff}, is given by:

$$l_{\mathrm{eff}} = (\pi n d^2 \mu^{1/2})^{-1} \qquad d = \frac{1}{2}(d_{\mathrm{air}} + d_{\mathrm{H_2SO_4}})$$

$$\mu = \frac{M_{\mathrm{air}}}{M_{\mathrm{air}} + M_{\mathrm{H_2SO_4}}}. \tag{14}$$

In the above expressions, d's are the diameters of the molecules and M's are the molecular weights. Let us finally recall that the Knudsen number is defined as:

$$\mathrm{Kn} = \frac{l_{\mathrm{eff}}}{r}. \tag{15}$$

To estimate dr/dN_A, Hamill et al. (1977b) used the following expression:

$$\frac{4}{3}\pi r^3 = N_A \upsilon_A + N_B \upsilon_B = \frac{N_A \overline{\upsilon}}{\chi}, \tag{16}$$

where $\overline{\upsilon}$ is the average volume per molecule, and

$$\chi = \frac{N_A}{N_A + N_B}. \tag{17}$$

If both $\overline{\upsilon}$ and χ are constant,

$$\frac{dr}{dN_A} = \frac{\overline{\upsilon}}{4\pi r^2 \chi}. \tag{18}$$

Finally,

$$\frac{dr}{dt} = \frac{\overline{\upsilon} D n_A}{r\chi(1 + \lambda \mathrm{Kn})} = \frac{\overline{\upsilon} D p_A / kT}{r\chi(1 + \lambda \mathrm{Kn})}. \tag{19}$$

To include the effect of evaporation, pressure p_A needs to be substituted by $p_A - p_A^0$.

The general dynamic equation for the condensational growth of the aerosol population can be written as (Brock 1972; Ramabhadran et al. 1976):

$$\frac{\partial n(V; t)}{\partial t} = -\frac{\partial}{\partial V}\left[\frac{dV}{dt} n(V; t)\right] + \mathcal{R}, \tag{20}$$

where $\mathcal{R}$ is the source term; here, the nucleation/conversion-to-nuclei source/sink. Let us rewrite (20) using (19):

$$\frac{\partial n(V; t)}{\partial t} = -\frac{\partial}{\partial V}\left[\frac{dr}{dt}\frac{dV}{dt} n(V; t)\right] = -\frac{\partial}{\partial V}\left[\underbrace{\frac{(4\pi)^{2/3}(3V)^{1/3}\overline{\upsilon} D(p_A - p_A^0)/kT}{\chi(1 + \lambda \mathrm{Kn})}}_{C(V)} n(V; t)\right] + \mathcal{R}. \tag{21}$$

We can also derive a similar form of equation for the distribution $\eta(U, V; t)$:

$$\frac{\partial \eta(V, U; t)}{\partial t} = -\frac{\partial}{\partial V}[C(V)\eta(V, U; t)] + \mathcal{R}. \tag{22}$$

It is easy to show that for both θ and ϵ, similar relationships apply.

For liquid aerosol with cores, the process of evaporation is more complicated because particles cannot evaporate below the core size. To derive the conversion rates from liquid aerosol with cores to solid particles, we start with the calculation of the rate of generation of aerosol droplets of the size equal to the core size—these are drops available for conversion. Let us write the finite-difference representation in V of (22) (for clarity of derivation, here we omit the dependence on time):

$$\frac{\partial \eta(V_j, U)}{\partial t} = -\frac{C(V_{j+1})\eta(V_{j+1}, U) - C(V_j)\eta(V_j, U)}{\underbrace{V_{j+1} - V_j}_{\Delta V_j}} \tag{23}$$

Then, let us integrate the above equation ($\int_0^{V_j} dU$, $U < V_j$):

$$\text{lhs} = \int_0^{V_j} \frac{\partial \eta(V_j, U)}{\partial t}\, dU = \frac{\partial n(V_j)}{\partial t}, \tag{24}$$

$$\begin{aligned}\text{rhs} &= \int_0^{V_j} \frac{C(V_{j+1})\eta(V_{j+1}, U) - C(V_j)\eta(V_j, U)}{\Delta V_j}\, dU \\ &= -\left[\int_0^{V_{j+1}} \frac{C(V_{j+1})\eta(V_{j+1}, U)}{\Delta V_j} - \int_0^{V_j} \frac{C(V_j)\eta(V_j, U)}{\Delta V_j}\, dU - \int_{V_j}^{V_{j+1}} \frac{C(V_{j+1})\eta(V_{j+1}, U)}{\Delta V_j}\right] \\ &= -\frac{C(V_{j+1})n(V_{j+1}, U) - C(V_j)n(V_j, U)}{\Delta V_j} - \frac{1}{2}[C(V_{j+1})\eta(V_{j+1}, U = V_{j+1}) + C(V_{j+1})\eta(V_{j+1}, U = V_j)]\frac{\Delta V_j}{\Delta V_j},\end{aligned} \tag{25}$$

where the trapezoidal rule was used to calculate one of the above integrals. Finally, we can write the rate with which liquid aerosol evaporates to the size of its cores as:

$$\mathcal{S}^n(V) = \frac{1}{2}[C(V^\Delta)\eta(V^\Delta, U = V^\Delta)V^\Delta + C(V^\Delta)\eta(V^\Delta, U = V)V], \tag{26}$$

where we introduce the notation $V^\Delta = V + \Delta V(V)$.

Not all aerosol drops ''available'' for conversion will actually do so. Because we have no information about the timescale of this process, we assume that the timescale of conversion is equal to that of nucleation. The sink for conversion is then $\mathcal{N}^{\text{hetero}}\mathcal{S}$, where $\mathcal{N}^{\text{hetero}}$ is defined in (9). Starting with distribution $\eta(V, U)$, the conversion rates for the moments, $\mathcal{N}^{\text{hetero}}\mathcal{S}^\theta$ and $\mathcal{N}^{\text{hetero}}\mathcal{S}^\epsilon$ can be obtained. In particular,

$$\mathcal{S}^\theta(V) = \frac{1}{2}[C(V^\Delta)\eta(V^\Delta, U = V^\Delta)V^\Delta + C(V^\Delta)\eta(V^\Delta, U = V)V], \tag{27}$$

$$\mathcal{S}^\epsilon(V) = \frac{1}{2}[C(V^\Delta)\eta(V^\Delta, U = V^\Delta)(V^\Delta)^2 + C(V^\Delta)\eta(V^\Delta, U = V)V^2]. \tag{28}$$

We can now write the equations for condensation and nucleation for two types of sulfuric aerosol and for two moments as:

$$\frac{\partial n(V; z, t)}{\partial t} = -\frac{\partial}{\partial V}[C(V)n(V; z, t)] + \begin{cases}\mathcal{N}^{\text{hetero}}\hat{n}(V; z, t) & \text{for } p_A > p_A^0 \\ \mathcal{N}^{\text{hetero}}\mathcal{S}^n(V) & \text{for } p_A < p_A^0,\end{cases} \tag{29}$$

$$\frac{\partial n_w(V; z, t)}{\partial t} = -\frac{\partial}{\partial V}[C(V)n_w(V; z, t)] + \begin{cases}\mathcal{J}^{\text{homo}} & \text{for } p_A > p_A^0 \\ 0 & \text{for } p_A < p_A^0,\end{cases} \tag{30}$$

$$\frac{\partial \theta(V; z, t)}{\partial t} = -\frac{\partial}{\partial V}[C(V)\theta(V; z, t)] + \begin{cases}\mathcal{N}^{\text{hetero}}V\hat{n}(V; z, t) & \text{for } p_A > p_A^0 \\ \mathcal{N}^{\text{hetero}}\mathcal{S}^\theta(V) & \text{for } p_A < p_A^0,\end{cases} \tag{31}$$

$$\frac{\partial \epsilon(V; z, t)}{\partial t} = -\frac{\partial}{\partial V}[C(V)\epsilon(V; z, t)] + \begin{cases}\mathcal{N}^{\text{hetero}}V^2\hat{n}(V; z, t) & \text{for } p_A > p_A^0 \\ \mathcal{N}^{\text{hetero}}\mathcal{S}^\epsilon(V) & \text{for } p_A < p_A^0.\end{cases} \tag{32}$$

The nucleation rate for $n(V; z, t)$ is based upon (9), whereas those for the moments can be easily derived by applying the appropriate integrations as defined in (1). For completeness, we also write the equation for solid particles with nucleation and conversion being, respectively, sink and source terms:

$$\frac{\partial \hat{n}(V; z, t)}{\partial t} \begin{cases}-\mathcal{N}^{\text{hetero}}\hat{n}(V; z, t) & \text{for } p_A > p_A^0 \\ -\mathcal{N}^{\text{hetero}}\mathcal{S}^n(V) & \text{for } p_A < p_A^0.\end{cases} \tag{33}$$

d. Condensation and evaporation of water vapor

When the environmental temperature and/or the water vapor partial pressure change, so does the equilibrium sulfuric acid mass fraction. In turn, this leads to the condensation or evaporation of water vapor. Let us first derive the expression for the rate of change of radius using the following assumptions: 1) mass of the core in a drop does not change; 2) mass of the H_2SO_4 fraction

also remains unchanged [here we follow Turco et al. (1979)]. If f is the core volume fraction, assumption 2 gives:

$$\frac{d}{dt}\left[\frac{4}{3}\pi r^3(1 - f)W\rho\right] = 0. \quad (34)$$

After derivation, we find that:

$$\frac{dr}{dt} = -\frac{r}{3}(1 - f)\frac{d\ \ln(W\rho)}{dt}. \quad (35)$$

Further, let us notice that

$$\frac{d}{dt} = \frac{\partial}{\partial t} + \mathbf{v}\cdot\boldsymbol{\nabla} = \left(\frac{\partial T}{\partial t} + \mathbf{v}\cdot\boldsymbol{\nabla}T\right)\frac{\partial}{\partial T} + \left(\frac{\partial p_W}{\partial t} + \mathbf{v}\cdot\boldsymbol{\nabla}p_W\right)\frac{\partial}{\partial p_W}. \quad (36)$$

Note that in our one-dimensional case in which we assume the standard atmosphere temperature profile, and the constant water vapor concentration profile, (36) has a simple form:

$$\frac{d}{dt} = \upsilon_z\frac{\partial}{\partial z}, \quad (37)$$

where υ_z represents different types of motion due to advection with the resolved flow, sedimentation, and eddy diffusion:

$$\upsilon_z = \underbrace{u_z}_{\text{advection}} + \underbrace{w}_{\text{sedimentation}} - \underbrace{E_D\frac{\partial\left(\ln\dfrac{n}{n_{\text{air}}}\right)}{\partial z}}_{\text{eddy diffusion}}. \quad (38)$$

In the above equation, υ_z represents the z-component of the velocity, w the terminal velocity, E_D the eddy diffusion coefficient, and n_{air} the concentration of air molecules. More details concerning transport processes can be found in the section dedicated to those processes.

Making use of (20) and (37), we can derive equations for the condensation of water vapor as:

$$\frac{\partial n(V)}{\partial t} = -\frac{\partial}{\partial V}\left\{-V\upsilon_z\frac{\partial\ \ln(W\rho)}{\partial z}\left[n(V) - \frac{\theta(V)}{V}\right]\right\}, \quad (39)$$

$$\frac{\partial \theta(V)}{\partial t} = -\frac{\partial}{\partial V}\left\{-V\upsilon_z\frac{\partial\ \ln(W\rho)}{\partial z}\left[\theta(V) - \frac{\epsilon(V)}{V}\right]\right\}, \quad (40)$$

$$\frac{\partial \epsilon(V)}{\partial t} = -\frac{\partial}{\partial V}\left\{-V\upsilon_z\frac{\partial\ \ln(W\rho)}{\partial z}\left[\epsilon(V) - \frac{\zeta(V)}{V}\right]\right\}, \quad (41)$$

where ζ is the third moment that can be calculated upon the knowledge of the first and second moments for the assumed form of the distribution function $\eta(V, U)$. Here $\upsilon^{\theta}{}_z$ and $\upsilon^{\epsilon}{}_z$ differ from υ_z, in particular,

$$\upsilon_z^{\theta} = \underbrace{u_z}_{\text{advection}} + \underbrace{w}_{\text{sedimentation}} - \underbrace{E_D\frac{\partial\left(\ln\dfrac{\theta}{n_{\text{air}}}\right)}{\partial z}}_{\text{eddy diffusion}}, \quad (42)$$

$$\upsilon_z^{\epsilon} = \underbrace{u_z}_{\text{advection}} + \underbrace{w}_{\text{sedimentation}} - \underbrace{E_D\frac{\partial\left(\ln\dfrac{\epsilon}{n_{\text{air}}}\right)}{\partial z}}_{\text{eddy diffusion}}. \quad (43)$$

Equations (20) and (37) lead us also to the equation for the homogeneous liquid drops ($f = 0$):

$$\frac{\partial n_w(V)}{\partial t} = -\frac{\partial}{\partial V}\left[-V\upsilon_z\frac{\partial\ \ln(W\rho)}{\partial z}n_w(V)\right]. \quad (44)$$

e. Coagulation

The mathematical treatment of the process of coagulation was developed by Smoluchowski (1917) for the case of Brownian coagulation. The equation describing the evolution of spectra, the kinetic coagulation equation, has the following form:

$$\frac{\partial n(V)}{\partial t} = \frac{1}{2}\int_0^V K(V', V_c)n(V', t)n(V_c, t)\,dV', - n(V, t)\int_0^{\infty} K(V, V')n(V', t)\,dV', \quad (45)$$

where K represents the coefficients (kernels) characterizing the nature of the process under consideration, and $V_c = V - V'$. For Brownian coagulation, the coagulation kernel for particles of two different sizes (denoted here ''1'' and ''2'') is (Pruppacher and Klett 1980):

$$K_{12} = 16\pi\overline{D}\overline{r}, \quad (46)$$

where $\overline{D} = (D_1 + D_2)/2$ and $\overline{r} = (r_1 + r_2)/2$; D denotes the diffusion coefficient and r the particle radius. The diffusion coefficient is:

$$D = kTB, \quad (47)$$

where B is the particle mobility (the ratio of the particle velocity to the force acting on the particle). The particle mobility with the correction introduced to the mobility obtained with the Stokes approximation is:

$$B = \left[1 + A\frac{l}{r} + Q\frac{l}{r}\exp\left(-\frac{br}{l}\right)\right]\Big/ 6\pi\eta r, \quad (48)$$

where η is the dynamic viscosity, l is the mean free path of gas molecules, and A, Q, and b are the coefficients that were obtained experimentally by Millikan (1923a,b). For highly dispersed aerosol (the apparent mean free path is much larger than the particle radius), as is the case with atmospheric aerosols, (46) was modified by Fuchs (1964):

$$K_{12} = 16\pi\overline{D}\bar{r}\beta; \tag{49}$$

the details how to calculate β can be found in Fuchs (1964, 288–295).

With the system of three different aforementioned types of aerosol, the coagulation equation requires a generalization. We do so with the help of the generalized distribution for all aerosol types, $\mathcal{E}(V, U)$; $0 \le U \le V$. After performing the integrations similar to those in section 2a, we arrive with the following expressions for the generalized concentration, and first and second moments:

$$N(V) = n(V) + \hat{n}(V) + n_w(V), \tag{50}$$

$$\mathcal{T}(V) = \theta(V) + \hat{n}(V)V \quad \text{and}$$

$$E(V) = \varepsilon(V) + \hat{n}(V)V^2. \tag{51}$$

Clearly, the first and second moments for purely liquid drops are equal to zero. Let us write the coagulation equation (45) for the distribution $\mathcal{E}(V, U)$, and then, let us perform the integration, $\int_0^V U\, dU^i$, $i = 0, 1, 2$. The resulting generalized coagulation equations are:

$$\frac{\partial n(V)}{\partial t} = \frac{1}{2}\int_0^V K(V', V_c)\Big\{n(V')[n(V_c) + \hat{n}(V_c) + n_w(V_c)] + \hat{n}(V')[n(V_c) + n_w(V_c)] + n_w(V')[n(V_c) + \hat{n}(V_c)]\Big\}\, dV' - n(V)\int_0^\infty K(V, V')[n(V') + \hat{n}(V') + n_w(V')]\, dV', \tag{52}$$

$$\frac{\partial \hat{n}(V)}{\partial t} = \frac{1}{2}\int_0^V K(V', V_c)\hat{n}(V')\hat{n}(V_c)\, dV' - \hat{n}(V)\int_0^\infty K(V, V')[n(V') + \hat{n}(V') + n_w(V')]\, dV', \tag{53}$$

$$\frac{\partial n_w(V)}{\partial t} = \frac{1}{2}\int_0^V K(V', V_c)n_w(V')n_w(V_c)\, dV' - n_w(V)\int_0^\infty K(V, V')[n(V') + \hat{n}(V') + n_w(V')]\, dV', \tag{54}$$

$$\frac{\partial \theta(V)}{\partial t} = \int_0^V K(V', V_c)\Big\{\theta(V')[n(V_c) + \hat{n}(V_c) + n_w(V_c)] + V'\hat{n}(V')[n(V_c) + n_w(V_c)] + n(V')[\theta(V_c) + V_c\hat{n}(V_c)] + \hat{n}(V')\theta(V_c) + n_w(V')[\theta(V_c) + V_c\hat{n}(V_c)]\Big\}\, dV' - \theta(V)\int_0^\infty K(V, V')[n(V') + \hat{n}(V') + n_w(V')]\, dV', \tag{55}$$

$$\frac{\partial \varepsilon(V)}{\partial t} = \int_0^V K(V', V_c)\Big\{\varepsilon(V')[n(V_c) + \hat{n}(V_c) + n_w(V_c)] + V'^2\hat{n}(V')[n(V_c) + n_w(V_c)] + n(V')[\varepsilon(V_c) + V_c^2\hat{n}(V_c)] + \hat{n}(V')\varepsilon(V_c) + n_w(V')[\varepsilon(V_c) + V_c^2\hat{n}(V_c)] + 2\theta(V')[\theta(V_c) + V_c\hat{n}(V_c)] + 2V'\hat{n}(V')\theta(V_c)\Big\}\, dV' - \varepsilon(V)\int_0^\infty K(V, V')[n(V') + \hat{n}(V') + n_w(V')]\, dV'. \tag{56}$$

During the derivation, we recognize that coagulation of a liquid drop containing core with a particle of any other type as well as coagulation of a homogeneous liquid drop with a solid particle results in a liquid drop containing core; and that a new solid particle and a new homogeneous liquid drop can be created only as an effect of coagulation of two particles or two drops, respectively.

3. Chemical processes leading to the production of aerosol

It is believed that the important precursor gases for H_2SO_4 are OCS, SO_2, and possibly, CS_2. These gases are transported from the troposphere to the stratosphere where OCS is transformed to SO_2, and SO_2 is oxidized

TABLE 1. Gas-phase reactions of sulfur compounds in the stratosphere.[a]

Reaction	Rate ($cm^3\ s^{-1}$)	Timescale (s)
1. $OCS + h\nu \rightarrow S + CO$		5×10^5
2. $OCS + O \rightarrow SO + CO$	$2.1 \times 10^{-11}\exp(-2200/T)$	1×10^6
3. $S + O_2 \rightarrow SO + O$	2.3×10^{-12}	1×10^{-5}
4. $SO + OH \rightarrow SO_2 + H$	8.6×10^{-11}	7×10^2
5. $SO + O_2 \rightarrow SO_2 + O$	$2.6 \times 10^{-13}\exp(-2400/T)$	3×10^0
6. $SO + ClO \rightarrow SO_2 + Cl$	2.8×10^{-11}	7×10^2
7. $SO_2 + OH \xrightarrow{M} HSO_3$	$3.0 \times 10^{-31}(T/300)^{-3.3}[M]$[b]	9×10^5
8. $SO_2 + h\nu \rightarrow SO_2 + O$		1×10^5
9. $HSO_3 + O_2 \rightarrow SO_3 + HO_2$	$1.3 \times 10^{-12}\exp(-330/T)$	1×10^{-4}
10. $SO_3 + H_2O \rightarrow H_2SO_4$	6.0×10^{-15}	5×10^1
11. $CS_2 + OH + 2O_2 \rightarrow OCS + HO_2 + SO_2$	$1.25 \times 10^{-16}\exp(4550/T)$ $[T + 1.81 \times 10^{-3}\exp(3400/T)]$	2×10^7
12. $CS_2 + O \rightarrow CS + SO$	$3.6 \times 10^{-12}\exp(-650/T)$	2×10^6

[a] The rates are taken from DeMoore et al. (1992).
[b] $[M]$ is the concentration of air molecules.

to H_2SO_4. In our calculation we include only those gas-phase chemical reactions that lead to the production of H_2SO_4. Here we follow closely Zhao et al. (1995). However, we add a couple of reactions involving CS_2. The reactions included in the model and their rates are listed in Table 1.

The continuity equations with appropriate chemical reaction terms according to Table 1 are solved for H_2SO_4, HSO_3, SO_3, SO_2, SO, S, OCS, and CS_2. The equation for H_2SO_4 contains the sink due to the aerosol production, and can be written as follows:

$$\frac{\partial n_A(z,\,t)}{\partial t} = k_k n_{\mathrm{HSO_3}}(z,\,t) n_W - \frac{\rho W}{m_A}(n_A(z,\,t) - n_A^0) \int_0^{V_{\max}} \underbrace{\frac{dV}{dt}}_{C(V)} [n(V;\,z,\,t) + n_w(V;\,z,\,t)]\,dV, \tag{57}$$

where k_k is the kinetic coefficient of reaction 10 in Table 1, $n_{\mathrm{HSO_3}}$ the concentration of HSO_3, and $V_{\max}$ the maximum volume of aerosol particles. Other species (O_2, O, H_2O, OH, and Cl) have the assumed vertical concentration profiles.

4. Transport processes

a. Advection and sedimentation

The aerosol particles under consideration are very small, the largest being of the order of 1 μm in radius. Their inertia is therefore so small that, with high accuracy, their movements are reduced to following fluid parcel trajectories and to sedimenting with their terminal velocities. Therefore, the advection of the aerosol concentrations can be written as follows:

$$\frac{\partial n(V;\,z,\,t)}{\partial t} = -\frac{\partial}{\partial t}\{[u_z(z) + w(V;\,z)]n(V;\,z,\,t)\} + \mathcal{M}^n, \tag{58}$$

where $u_z(z)$ is the velocity of the resolved flow, $w(V;\,z)$ is the sedimentation velocity, and $\mathcal{M}^n$ is the source–sink term. The unresolved scales of motion are represented by the eddy diffusion which will be described later.

The terminal velocity for small particles (with the molecular effects included) was calculated by Kasten (1968) as:

$$w = \frac{2}{9}\frac{\rho r^2 g}{\eta}\left[1 + A\frac{l}{r} + Q\frac{l}{r}\exp\left(-\frac{br}{l}\right)\right]. \tag{59}$$

In the above equation, we assumed that the density of air is much smaller than that of the aerosol, and that the density of cores and nuclei is equal to the aerosol density.

The advection equations for the nuclei and homogeneous drops have the same form as that for the aerosol with cores [i.e., (58)]; therefore, they will not be listed here. Note also that we can formally rewrite (58) for the distribution function $\eta(V,\,U)$, and after performing the usual integrations ($\int_0^V U\,dU$ and $\int_0^V U^2\,dU$), we arrive with the equations for the advection of the first and second moments:

$$\frac{\partial \theta(V; z, t)}{\partial t} = -\frac{\partial}{\partial z}\{[u_z(z, t) + w(V; z)]\theta(V; z, t)\} + \mathcal{M}^{\theta}, \quad (60)$$

$$\frac{\partial \epsilon(V)}{\partial t} = -\frac{\partial}{\partial z}\{[u_z(z, t) + w(V; z)]\epsilon(V; z, t)\} + \mathcal{M}^{\epsilon}. \quad (61)$$

The source/sink term in (58) is obtained by applying the downward control principle (Haynes et al. 1990) to estimate the mean meridional circulation. For the residual mean velocities u_z (vertical) and u_m (meridional) one can write the mass continuity equation in spherical coordinates as follows (Andrews et al. 1987):

$$\frac{1}{a\cos\phi}\frac{\partial}{\partial\phi}(u_m\cos\phi) + \frac{1}{\rho_{\text{air}}}\frac{\partial}{\partial z}(\rho_{\text{air}}u_z) = 0, \quad (62)$$

where ϕ is the geographical latitude, and a is the earth's radius. Thus, the meridional source/sink is

$$\mathcal{S}(z) = 2n(V; z, t)\frac{1}{a\cos\phi}\frac{\partial}{\partial\phi}(u_m\cos\phi) = -2n(V; z, t)\frac{1}{\rho_{\text{air}}}\frac{\partial}{\partial z}(\rho_{\text{air}}u_z). \quad (63)$$

In the above equation, factor two is used to accommodate the meridional sink in both directions north and south. The expression for the meridional source/sink is identical for all the particulate and chemical species. Note that (58) applies to all modeled chemical species as well.

b. Eddy diffusion

The standard diffusion equation for a two-phase flow composed, in this particular case, of aerosol and air is

$$\frac{\partial[n(V; z, t)M(V)]}{\partial t} = \frac{\partial}{\partial z}\left\{E_D[n(V; z, t)M(V) + n_{\text{air}}M_{\text{air}}]\frac{\partial}{\partial z}\frac{n(V; z, t)M(V)}{n(V; z, t)M(V) + n_{\text{air}}M_{\text{air}}}\right\}, \quad (64)$$

where $M(V)$ and M_{air} are the masses of aerosol particles and air molecules, respectively, and E_D is the eddy diffusion coefficient. Because $n(V)M(V) \ll n_{\text{air}}M_{\text{air}}$, after a few simple algebraic steps, we have the following form of the diffusion equation for the aerosol with cores:

$$\frac{\partial n(V; z, t)}{\partial t} = \frac{\partial}{\partial z}\left[E_D n_{\text{air}}\frac{\partial}{\partial z}\frac{n(V; z, t)}{n_{\text{air}}}\right]. \quad (65)$$

We tacitly assume here that the eddy diffusion coefficient is species-independent. The diffusion equations for other variables ($\hat{n}$, n_w, θ, and ϵ) have forms identical to the above. The derivation of the diffusion equations for the moments proceeds along the same line as that for the advection equations.

To incorporate eddy diffusion in the equation describing condensation of water vapor, we need a form of the diffusion equation that defines the diffusional velocity. This is

$$\frac{\partial n(V; z, t)}{\partial t} = -\frac{\partial}{\partial z}\left\{\underbrace{\left[-E_D\frac{\partial}{\partial z}\ln\frac{n(V; z, t)}{n_{\text{air}}}\right]}_{\text{Diffusion Velocity}}n(V; z, t)\right\}. \quad (66)$$

In our model we use different physical meaning as well as values of the eddy diffusion coefficient from those commonly in use in one-dimensional models. We assume that eddy diffusion represents turbulent mixing, and not the combined effects all horizontal and vertical motions. We represent motion in the stratosphere as latitudinally averaged. Vertical motion is represented by an explicit velocity field, whereas meridional motion is represented by a meridional sink/source for each chemical species and particulate. The vertical diffusion coefficient is obtained from measurements of the rate of energy dissipation in the stratosphere (Lilly et al. 1974) as:

$$E_D = \frac{\epsilon}{3N^2} \quad (67)$$

where ϵ is the rate of energy dissipation, and N is the Brunt-Väisälä frequency;

$$N^2 = \frac{g}{z}\frac{\partial\vartheta}{\partial z}, \quad (68)$$

ϑ being the potential temperature. The eddy diffusion coefficient is plotted in Fig. 1a.

5. Design of a numerical experiment

For our experiment, we choose a domain representing the equatorial circle (15°S–15°N) from the tropopause up to 40 km. The meteorological parameters such as temperature, pressure, and air density have constant ver-

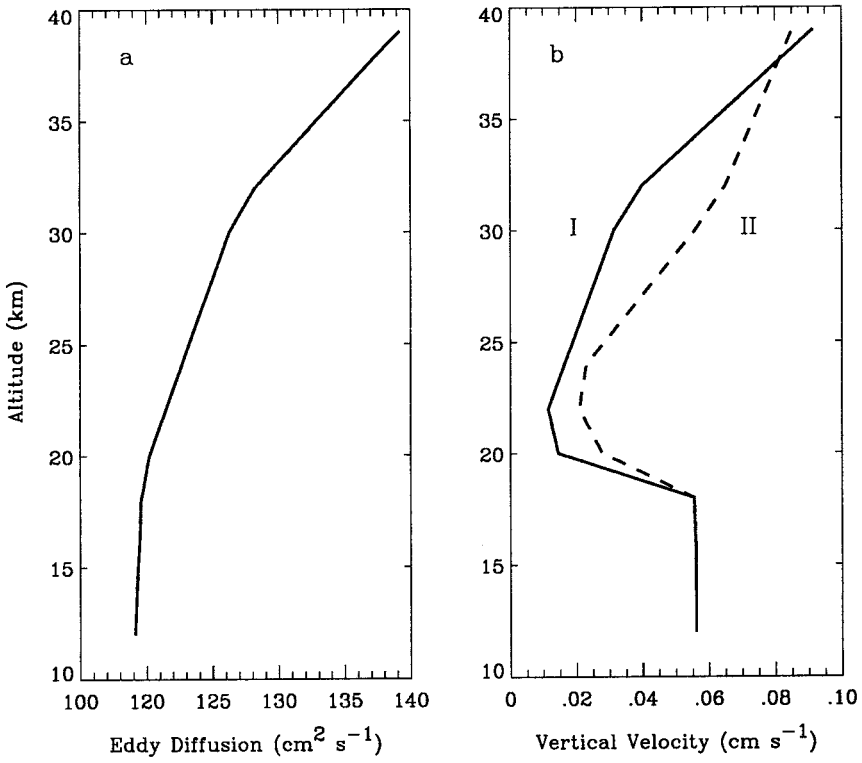

FIG. 1. Vertical profile of the eddy diffusion coefficient (a). Vertical profiles of the vertical velocity used in calculations (b).

tical profiles according to the standard atmosphere. A constant profile of the water vapor concentration was obtained from Sissenwine et al. (1968). Chemical species not integrated by our model are also assumed to have constant concentration profiles. In particular, ozone concentration was obtained from measurements (Krueger and Minzner 1976) and concentrations of O, OH, HO_2, ClO, and NO_2 from numerical modeling (Brasseur and Solomon 1986).

For the quiescent stratosphere, the chemical and physical processes are driven by the influx of OCS, SO_2, and CS_2; and Aitken nuclei from the troposphere. In the calculations, we assume the lognormal profile of Aitken nuclei at the bottom of the stratosphere:

$$\hat{n}(r) = F_{LN}(r; A_0, \xi_0, \sigma_0) = \frac{A_0}{\sqrt{2\pi}\,\sigma_0 r} \exp\left[-\frac{(\ln r - \ln\xi_0)^2}{2\sigma_0^2}\right], \quad (69)$$

with $A_0 = 200$ particles per cm^3, $\xi = 0.01$ μm, and $\sigma_0 = 0.1$. We assume the constant concentrations of OCS, SO_2, and CS_2 at the bottom of the domain. These are 0.4, 0.2, and 0.06 ppb, respectively, for OCS, SO_2, and CS_2. The mechanism that transports species to the stratosphere is based on the estimates of the global troposphere–stratosphere exchange. In particular, we use a constant vertical velocity profile that represents a long time average of the upward velocity over the equator. [The velocity profile was estimated upon the mass streamfunction calculated by Rosenlof and Holton (1993).] This rather rough estimate of the vertical velocity profile was later modified in order to examine the model sensitivity to this parameter. The meridional sink/source is calculated accordingly upon the mass continuity equation. Other species have zero initial concentrations.

We emphasize the fact that for the volcanic case the interpretation of what our model represents differs substantially from that for the undisturbed stratosphere. Until the gases and particulates emitted by a volcano became well mixed over the entire globe (and then the interpretation is the same as that for the quiescent stratosphere), the modeled concentrations represent the areas affected by the emission. We tacitly assume that in that region all species are well mixed. Although this assumption is commonly used in modeling, it is not correct, and the obtained results cannot be trusted but in a qualitative way. In order that the dilution of the volcanic material be accounted for, each of the modeled species has an additional sink due to dilution with the background stratosphere. In this we follow Zhao et al. (1995). We assume that horizontal dilution takes place in the first 30 days in low latitudes covering one third of the total earth area, and then, up to 365 days in the entire atmosphere. After one year, the dilution term is not needed, and modeling proceeds in exactly the same

way as for the nonvolcanic case. To account for dilution, we assume that for each species the product of concentration and the area where the dilution of the ''clean'' and ''volcanic'' air already took place is constant. Then, we can write for an arbitrary species:

$$\frac{\partial n}{\partial t} = \frac{\partial}{\partial t}\left(\frac{n(t_0)S(t_0)}{S(t)}\right) = -\frac{1}{S^2(t)}\frac{\partial S(t)}{\partial t}n(t_0)S(t_0), \tag{70}$$

where n is the concentration of a species, $S(t)$ is the area of the volcanic cloud, and $n(t_0)$ and $S(t_0)$ are the same quantities at a reference time instant; here $t_0 = t - \Delta t$; Δt being the time step for advection modeling. Zhao et al. assume $S(t)$ in the following form:

$$S(t) = S(t_0) + \frac{\partial S(t)}{\partial t}\Delta t, \tag{71}$$

where

$$\frac{\partial S(t)}{\partial t} = \begin{cases} 0.5S_{\text{in}} \text{ per day} & \text{for } t \le 30 \text{ days} \\ 0.1S_{\text{in}} \text{ per day} & \text{for } 30 \text{ days} < t \le 365 \text{ days.} \end{cases} \tag{72}$$

In the above equation, S_{in} denotes the initial area of the volcanic cloud equal to 10^7 km^2. Note that it is assumed that the volcanic cloud dilutes at the same rate at all altitudes.

For the volcanic case, we assume that the initial amounts of SO_2 and volcanic ash injected into the atmosphere are equal to those emitted during the 1991 Mount Pinatubo eruption. After Zhao et al. (1995) these are 20 Mt of SO_2, and 40 Mt of volcanic ash with the bimodal lognormal size distribution:

$$\hat{n}(r) = \sum_{i=1}^{2} \frac{A_i}{\sqrt{2\pi}\,\sigma_i r} \exp\left[-\frac{(\ln r - \ln\xi_i)^2}{2\sigma_i^2}\right], \tag{73}$$

where $\xi_1 = 0.5$ μm, $\xi_2 = 3$ μm, $\sigma_1 = 0.125$, and $\sigma_2 = 0.2$. The normalization coefficients A_i were chosen in such a way that 2.5% of mass is in the first mode, and 97.5% in the second mode. All the injected mass was uniformly distributed between 20 and 30 km.

6. Numerical procedures

The physical processes described in sections 2–4 are characterized by different timescales as well as described by different types of equations: hyperbolic equations for condensation and advection, elliptic equation for diffusion, and integro–differential equation for coagulation. Therefore, we have to apply various methods of solution suitable for different processes.

The domain of integration and the boundary and initial conditions are determined as follows. For the aerosol, we have a two-dimensional domain, Ω (the particle volume and the altitude being the coordinates), and for chemical species a one-dimensional domain, Ξ (the altitude). The particle volume changes from this corresponding to 0.0001-μm radius to that corresponding to 100 μm, whereas the altitude is from 12 to 40 km (levels z_0 and $z_{\max}$, respectively). The discretization in the direction of the particle volume is performed in the transformed coordinate J defined as:

$$V = V_0 \mathcal{G}^{J-1}, \tag{74}$$

where V_0 is the minimum volume, and $\mathcal{G} = \sqrt{2}$. The above transformation facilitates the calculation of the coagulation integrals. Let us denote the lower and upper limits of the J domain by J_0 and $J_{\max}$, respectively. With this notation, the boundary conditions are:

$$\forall (J, z, t) \in \partial\Omega|_{J=J_0, J=J_{\max}} \quad \mathcal{A}(J, z, t) = 0 \tag{75}$$

$$\forall (J, z, t) \in \partial\Omega|_{z=z_0} \quad \begin{cases} \mathcal{A}(J, z, t) = \text{const (lognormal)} & \text{for } \hat{n} \\ \partial\mathcal{A}(J, z, t)/\partial t = 0 & \text{otherwise} \end{cases} \tag{76}$$

$$\forall (J, z, t) \in \partial\Omega|_{z=z_{\max}} \quad \begin{cases} \partial\mathcal{A}(J, z, t) = 0 & \text{for quiescent case} \\ \mathcal{A}(J, z, t) = \text{const (background)} & \text{for volcanic case} \end{cases} \tag{77}$$

$$\forall (z, t) \in \partial\Xi|_{z=z_0} \quad \begin{cases} \mathcal{V}(z, t) = \text{const} & \text{for species from troposphere} \\ \partial\mathcal{V}(z, t)/\partial t = 0 & \text{otherwise} \end{cases} \tag{78}$$

$$\forall (z, t) \in \partial\Omega|_{z=z_{\max}} \quad \begin{cases} \partial\mathcal{V}(z, t)/\partial t = 0 & \text{for quiescent case} \\ \mathcal{V}(z, t) = \text{const (background)} & \text{for volcanic case,} \end{cases} \tag{79}$$

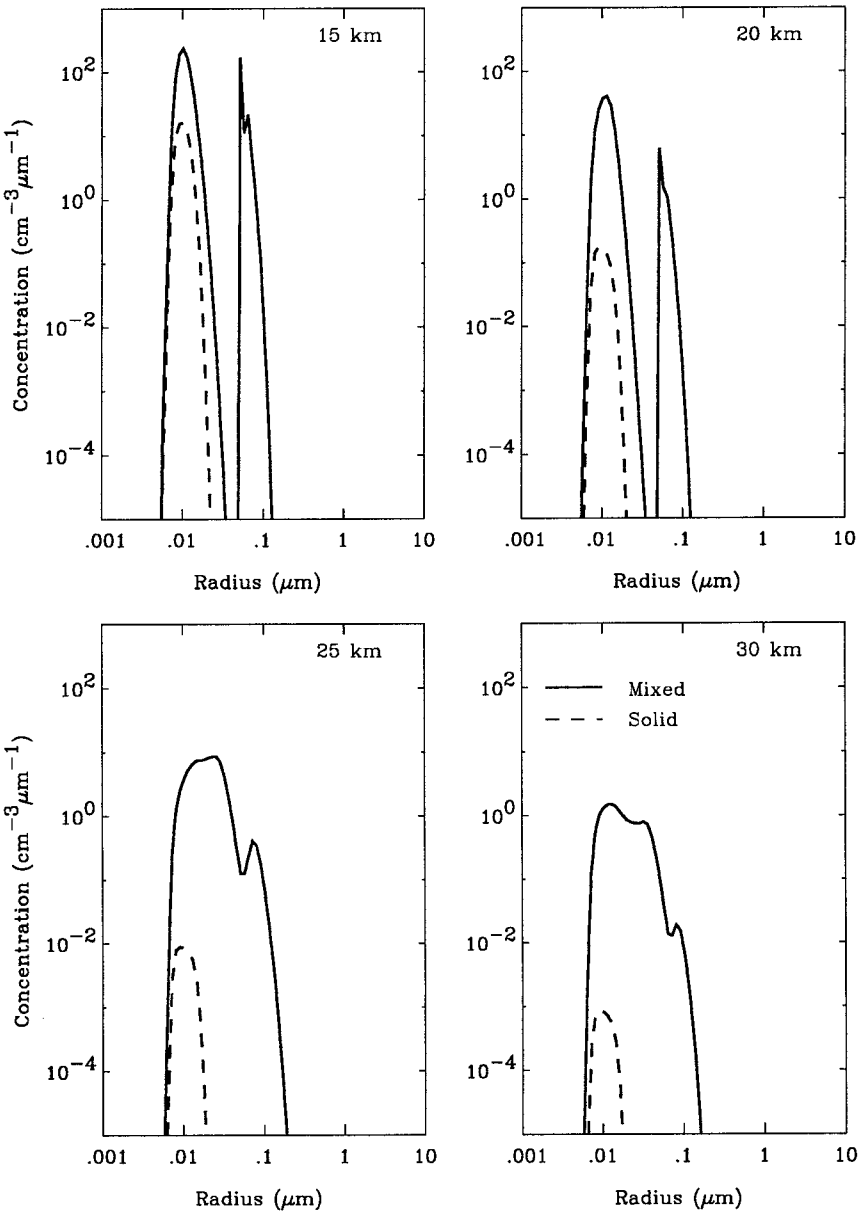

FIG. 2. Size distribution of Aitken nuclei and liquid aerosol with cores for the quiescent period case (scenario with OCS) at 15, 20, 25, and 30 km of altitude.

where $\partial\Omega$ and $\partial\Xi$ denote the domain boundaries, $\mathcal{A}$ the aerosol species and the moments, and $\mathcal{V}$ the gaseous species. The initial condition for the quiescent stratosphere case consisted of zero concentrations for the first run. Later, the results taken from previous runs initialized the model. For the volcanic case, additional SO_2 and volcanic ash amounts were added in the form of the initial conditions (these are described in the previous section).

A variety of numerical methods were applied. To solve the equation describing condensation/evaporation of sulfuric acid with nucleation/conversion as a source/sink term as well as the advection equation with source/sink terms describing meridional motion and dilution, the positive definite advection scheme with small implicit diffusion was applied (Smolarkiewicz and Grabowski 1989). Note that both aforementioned processes are described by the same type of equation. The same positive advection scheme was also modified to solve the equation describing the condensation of water vapor. For Aitken nuclei and volcanic ash, the analytic solution was applied for the case of nucleation, whereas the Euler forward scheme was applied for conversion. The integrals in the coagulation equations were calculated with the help of the Gauss–Legendre quadrature, and the equations were integrated using the explicit Euler for-

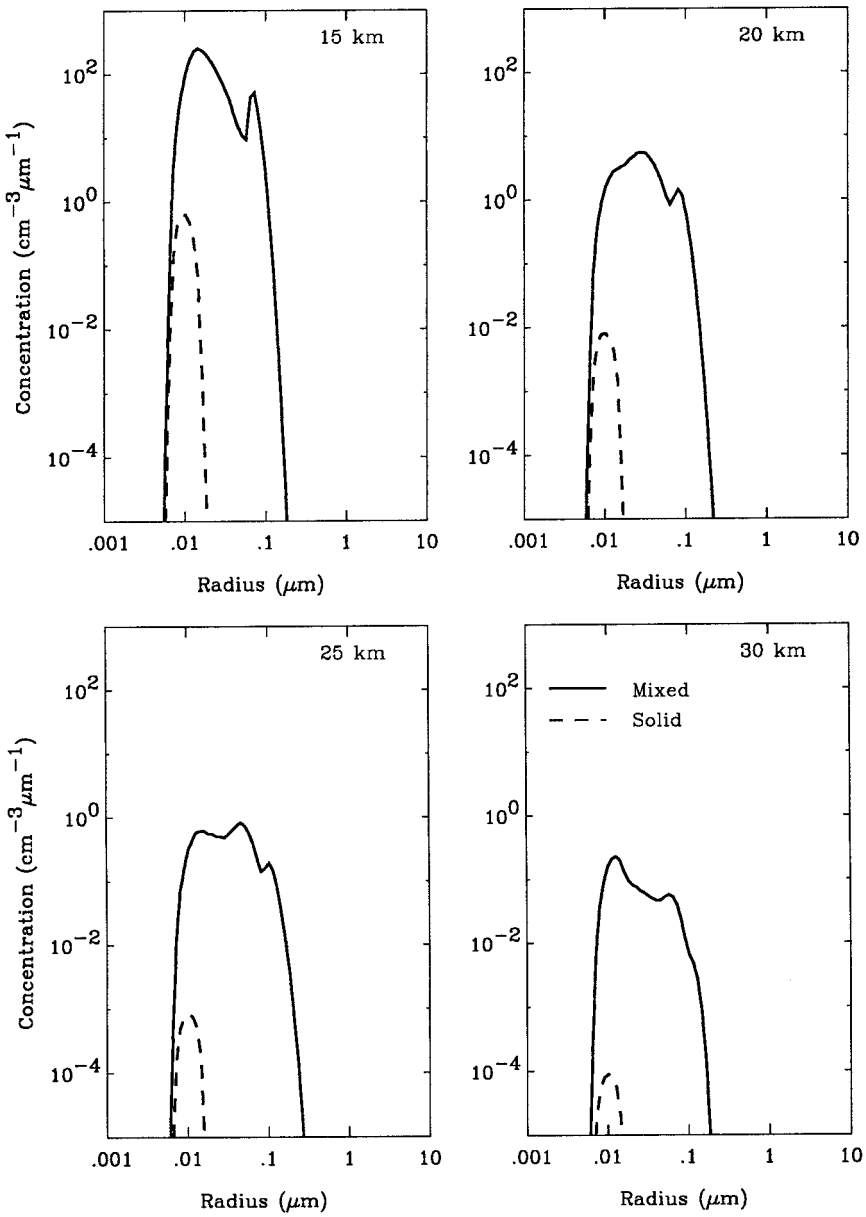

FIG. 3. Size distribution of Aitken nuclei and liquid aerosol with cores for the quiescent period case (scenario with OCS and CS_2) at 15, 20, 25, and 30 km of altitude.

ward scheme. The diffusion equation was solved according to the implicit Crank–Nicolson method. The chemical kinetic calculations, because of their stiff behavior, were divided into three groups according to their timescales (see Table 1). Then, steady-state solution, analytic solution, and Euler forward method were used for fast, intermediate, and slow reactions, respectively (Brasseur and Mandronich 1995).

The solution was carried out on 29 vertical levels, and 128 (quiescent stratosphere) or 140 (volcanic case) particle size grid points. Because of significant differences in timescales of different processes, it was necessary to solve the entire system with time splitting. Usually, two different time steps were used. Generally, the time step for condensation/evaporation of sulfuric acid, nucleation, diffusion, and chemical kinetic calculations was of the order of several seconds, whereas that for advection, condensation/evaporation of water vapor, and coagulation was of the order of a few minutes.

7. Results

For the quiescent stratosphere case, we selected two different vertical velocity profiles (see Fig. 1b), and three different scenarios of supplying H_2SO_4 precursors

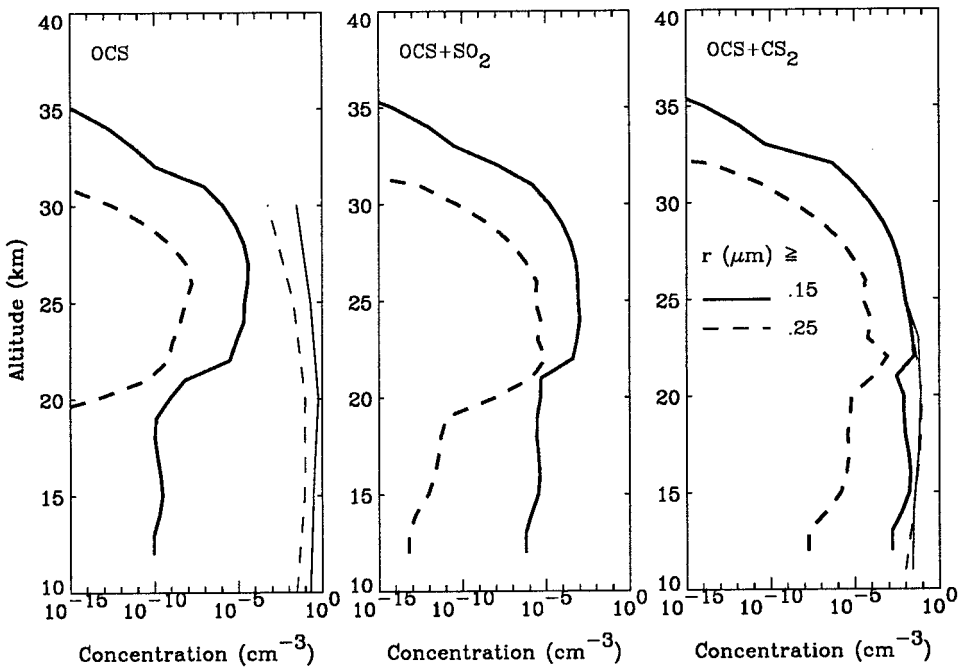

FIG. 4. Vertical profiles of the total number of particles of radii greater than or equal to 0.15 and 0.25 μm for three quiescent scenarios (OCS, OCS and SO_2, and OCS and CS_2). For comparison, the left panel shows the measured concentrations from Hoffman and Rosen (1981) (Laramie, autumn/winter 1978/79), and the right panel shows the measured concentrations from Junge et al. (1961) (1959/60).

to the stratosphere. In the first scenario, only OCS was injected into the stratosphere. Recall that a constant flux of the species was obtained by assuming a constant value of the species concentration as well as of the vertical velocity at the bottom of the z domain. OCS alone did not provide satisfactory results, in particular, the concentration of large aerosol droplets and SO_2 seemed to be too low. Therefore, the SO_2 source from the troposphere was added. The results were also nonsatisfactory (too low concentrations of large particles), and in the third scenario, CS_2 replaced SO_2. In the third scenario, the concentration of SO_2 produced at the bottom of the domain was sufficiently high, and consequently, no experiments with sources of all three gases were performed.

In Figs. 2 and 3, we present the concentrations of two types of the modeled aerosol, Aitken nuclei and drops with solid cores at four altitudes, respectively, for the first and third scenario with velocity profile I. The concentration of homogeneous liquid aerosol is too low to show up in Figs. 2 and 3. It can be seen that in the first scenario (Fig. 2), because of lower levels of H_2SO_4, the spectrum of liquid aerosol with cores, which is the dominant mode, is bi-modal. The first mode is due to forcing of Aitken nuclei and the second is due to condensational growth of nucleated aerosol. In the third scenario (Fig. 3), these two modes are barely distinguishable.

In Figs. 4 and 5, respectively, the vertical concentration profiles of the total aerosol (all three types) of radii greater than or equal to 0.15 and 0.25 μm, and the ratio of the concentration of aerosol $r \geq 0.15$ μm to that of aerosol $r \geq 0.25$ μm are plotted for all three scenarios. In Fig. 4, the aerosol levels are lower than those measured by Hoffman and Rosen, and also by Junge (Hoffman and Rosen 1981); we will comment on that later. The maximum of the concentration is reached relatively high (approximately at 22–25 km), which is consistent with the fact that the model represents the equatorial region by assuming a particular velocity profile. Turning attention to Fig. 5, one can observe that our model possesses the ability to capture the decrease in the ratio of concentration above 30 km. [The inability of other models to capture this effect was discussed by Hoffman and Rosen (1981).] For comparison, in the same figure we show the concentration ratio for the volcanic case 1 yr after the eruption. The latter profile resembles more measurements (Hoffman and Rosen 1981), which suggests that in the real stratosphere the aerosol levels are maintained by both influx of sulfur-bearing gases during quiescent periods and volcanic activity. [Note that the visible disagreement in the lower altitudes between our profiles and that by Hoffman and Rosen (1981) is a consequence of using a particular velocity profile in our calculation, whereas the experimental profile represents an average of many measurements.]

We also found that, to a certain extent, the aerosol concentrations depend on a particular velocity profile. The comparison of the vertical profiles of the concentration for vertical velocity profiles I and II illustrates this fact (see Fig. 6).

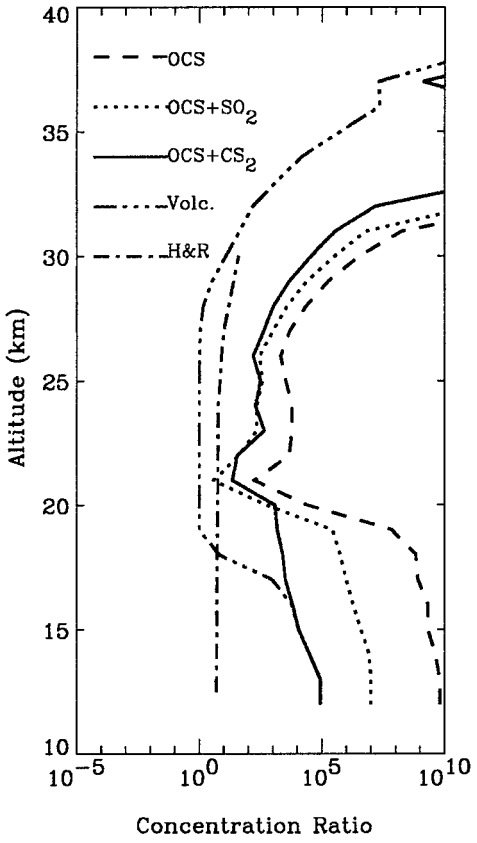

FIG. 5. Vertical profiles of ratios of concentration of particles of radii greater than or equal to 0.15 to that of particles of radii greater than or equal to 0.25 μm for three quiescent scenarios (OCS, OCS and SO_2, OCS and CS_2), for the volcanic case, and from Hoffman and Rosen (1981).

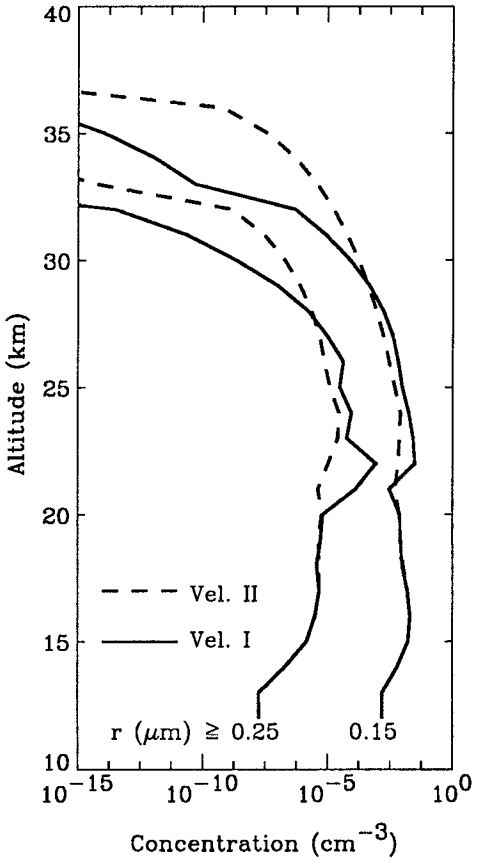

FIG. 6. Vertical profiles of the total number of particles of radii greater than or equal to 0.15 and 0.25 μm (scenario with OCS and CS_2) for two different vertical velocity profiles.

In the volcanic case we applied velocity profile I, with the scenario with OCS and CS_2 being a constant in time tropospheric source. The details describing how the volcanic eruption was included in our model can be found in section 5. In Figs. 7a–d, the concentrations of three types of aerosol are plotted for different time instants up to five years after the eruption (1 day, 30 days, 1 yr, and 5 yr). Various modes can be recognized. Starting from the smallest particle sizes, we have the nucleation mode due to forcing of Aitken nuclei (0.01 μm, visible, e.g., 5 yr after the eruption at higher altitudes). The mode due to condensational growth of Aitken nuclei lies between 0.08 and 0.1 μm. Immediately after the eruption (up to one month), the nucleation modes on volcanic ash are present (0.5 and 3.0 μm). These two modes disappear through sedimentation. Finally, a maximum can be observed between 0.4 and 0.6 μm (depending on the altitude and the time instant after the eruption). The latter one can be attributed to the growth of aerosol nucleated on volcanic material and to the growth of nuclei generated in the process of homogeneous nucleation (e.g., 30 days, 30 km and 1 yr, 20 km). The two growth modes (0.08–0.1 and 0.4–0.6 μm) were observed by Deshler et al. (1993). The appearance of high concentrations of homogeneous liquid aerosol due to growth of homogeneous nucleation mode caused by the buildup of H_2SO_4 (one month after the eruption) is supported by observations (Hoffman and Rosen 1984). In our model, the abundance of homogeneous liquid aerosol appears a few days after the eruption at around 30-km altitude, and as the time progresses, ascends to lower levels, to finally disappear at 20-km altitude approximately 18 months later. Our modeled results suggest that this behavior is associated with the removal of large aerosol particles generated on volcanic ash. With time, large particles of both aerosol with cores and homogeneous liquid aerosol are removed via sedimentation. As it happens, no new ash particles are injected so the heterogeneous nucleation slows down. In the meantime, homogeneous nucleation remains unchanged making the growth of homogeneous drops more competitive. Eventually, the levels of H_2SO_4 are depleted, and no new homogeneous drops are formed whereas the ''old'' ones are removed by coagulation and sedimentation.

The interesting features are observed on the vertical

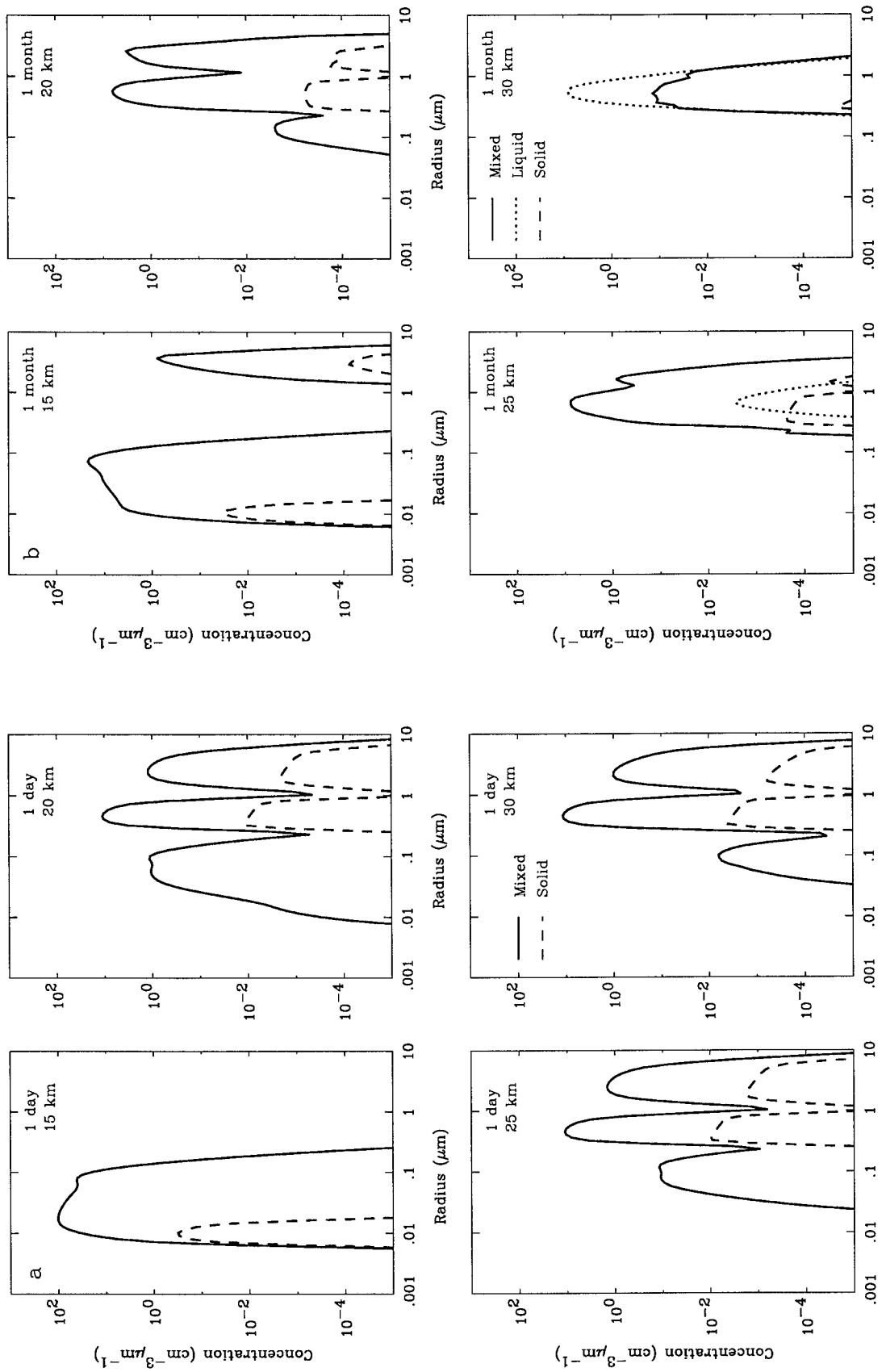

FIG. 7. Size distribution of liquid aerosol with cores, homogeneous liquid aerosol, and solid particles for the volcanic case: (a) 1 day, (b) 1 month, (c) 1 yr, and (d) 5 yr after the eruption at 15, 20, 25, and 30 km of altitude.

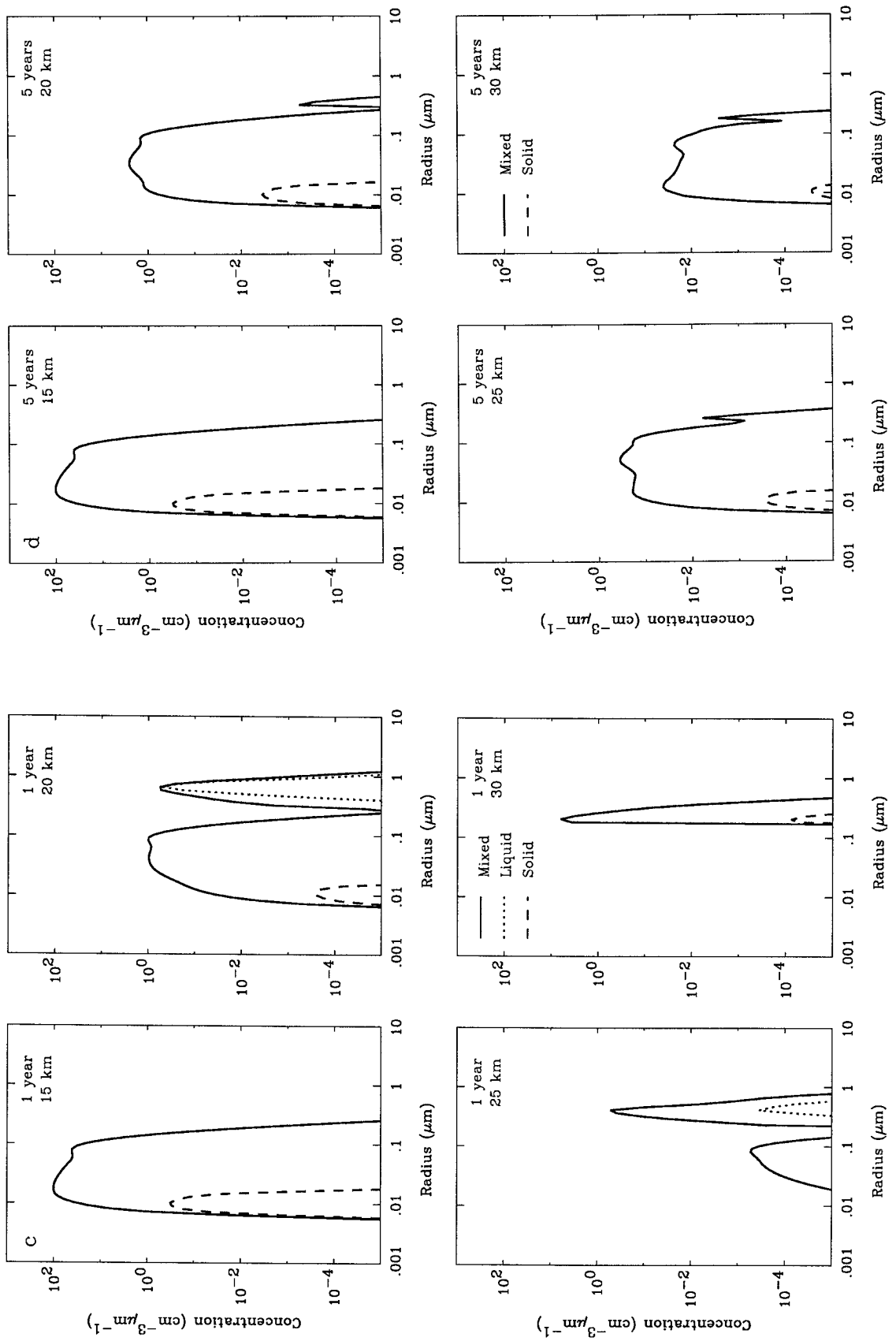

FIG. 7. (*Continued*)

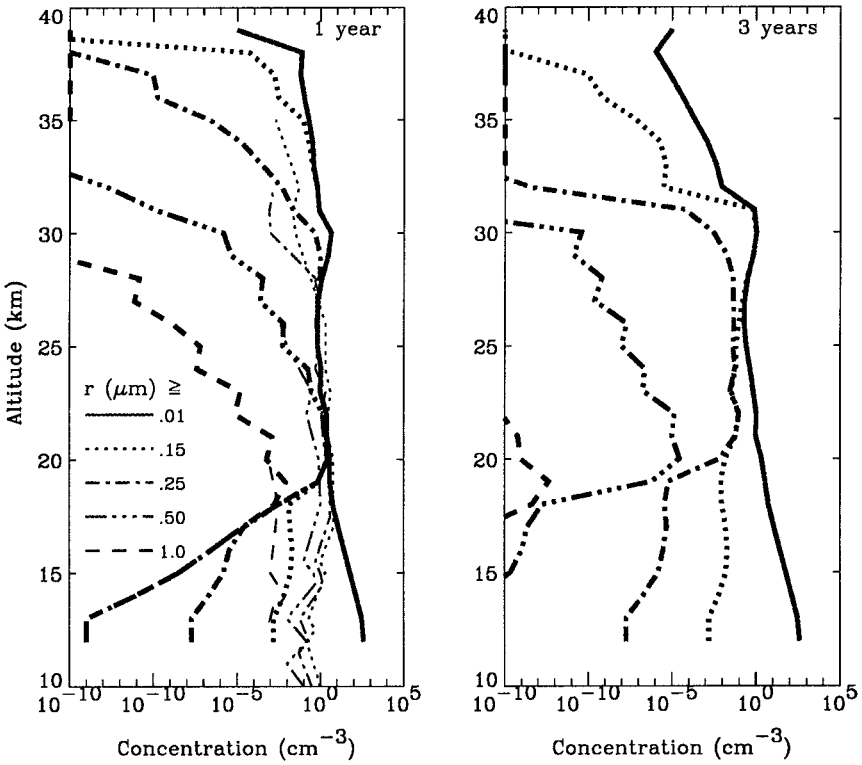

FIG. 8. Vertical profiles of the total number of particles of radii greater than or equal to 0.01, 0.15, 0.25, 0.50, and 1.00 μm 1 yr and 3 yr after the eruption. For comparison, the left panel shows the measured concentrations (thin lines) for Laramie from 24 June 1992 (1 yr after the eruption of Mount Pinatubo) from Deshler et al. (1993).

profiles of the aerosol concentrations. Figure 8 shows the vertical profiles of the concentration of the total aerosol of radii greater than or equal to 0.01, 0.15, 0.25, 0.5, and 1 μm. Figure 9 shows the vertical profiles of all three types of aerosol. Two maxima can be observed at 20 and 30 km. The lower maximum of the aerosol of radii greater than or equal to 0.15, 0.25, 0.5, and 1 μm coincides with that of homogeneous liquid aerosol. Thus the process of condensation seems to be responsible for the creation of this maximum. The other maximum, for the total aerosol of radii greater than or equal to 0.01. 0.15, and 0.25 μm is located at altitudes corresponding to the transition from the nucleation–condensation regime to that of conversion–evaporation. We propose the following mechanism for the generation of this maximum. At altitudes close to the saturation level of H_2SO_4, either the condensational growth is slow or evaporation and conversion to solid particles takes place. Therefore, ''fast'' sedimenting droplets are created at a much slower rate than, say, at 20 km. Further, because of the presence of volcanic ash (solid particles), the evaporation to smaller and smaller drops, as is the case with homogeneous liquid aerosol, is not present. These two processes facilitate the accumulation of drops close to the level of saturation. Note that the assumed vertical velocity profile (i.e., increase of the upward velocity with height) additionally enhances the accumulation. The maximum due to transition from nucleation–condensation to conversion–evaporation is a long lasting one: it disappears after approximately 5 yr.

In Fig. 8, the results were superimposed with the experimental data obtained by Deshler et al. (1993). The measurements were taken in Larami, Wyoming, on 24 June 1992; 1 yr after the eruption of Mount Pinatubo. The agreement seems to be particularly good between 18 and 25 km of altitude where the processes responsible for the formation of aerosol are related to the physics of the aerosol (e.g., condensation, coagulation). The agreement is poor at lower altitudes. This can be easily explained by meteorological and dynamical factors. In our calculation, we assumed the standard atmosphere temperature profile as well as an arbitrary velocity field, which characterizes the equatorial region and not midlatitudes. Still we think that the comparison is very favorable—we attribute it to a proper modeling of the physics of the aerosol.

We found that the effect of the volcanic eruption on the aerosol population is very persistent. The concentration of H_2SO_4 returns to the background or steady-state level after approximately 5 yr, whereas the concentrations of aerosol of radii greater than or equal to 0.15 μm and 0.25 μm is still higher than that of the background level. Even after

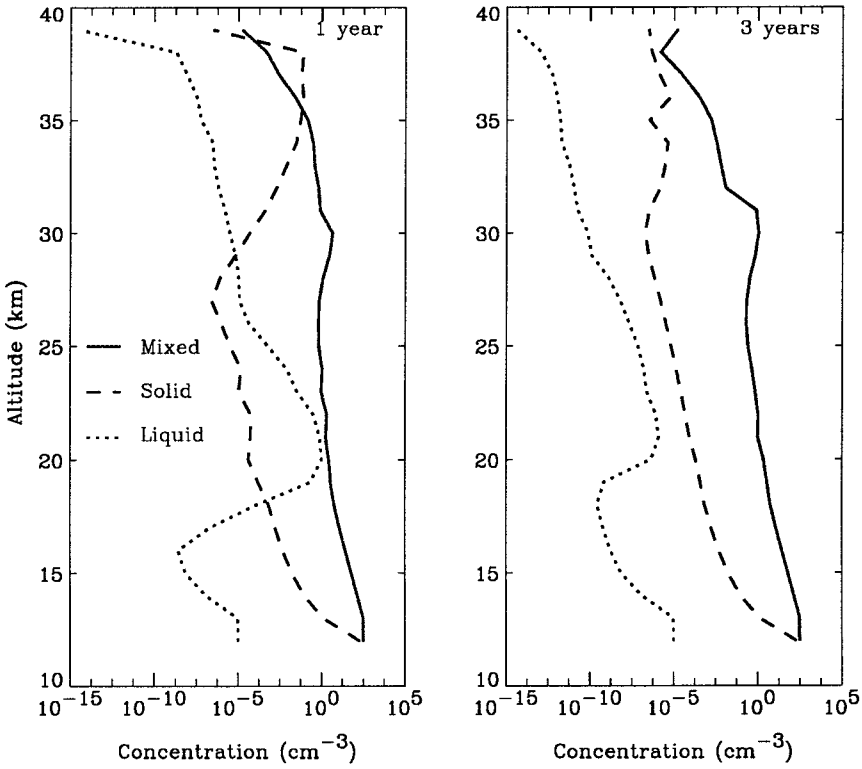

FIG. 9. Vertical profiles of liquid aerosol with cores, homogeneous liquid aerosol, and solid particles 1 yr and 3 yr after the eruption.

6 yr, at certain altitudes the concentration of the particles $r \geq 0.25$ μm is elevated by two orders of magnitude (see Fig. 10), which leads to the conclusion that smaller particles are removed faster than the larger ones. (Note that all particles discussed here are in the submicron range. Therefore, microphysical processes rather than sedimentation contribute to the particle removal by shifting them up or down the size scale.) The effect is also present for aerosol of radii greater than or equal to 0.5 μm. This could explain measurements performed by Junge et al. during 1959 and 1960, and by Hoffman and Rosen during 1979 (Hoffman and Rosen 1981). They noted that while the concentrations of the particles $r \geq 0.15$ μm in 1979 were higher than those in 1959–60, the concentrations of particles $r \geq 0.25$ μm remained unchanged. (Both periods when the measurements were taken are considered to be quiescent periods.) The difference in the aerosol levels was attributed to the eruption of Mt. Agung on Bali (8°S) in 1963. We hypothesize that in 1959–60 particles $r \geq 0.15$ μm were close to the steady-state equilibrium, whereas those $r \geq 0.25$ μm did not yet reach that state. On the other hand, in 1979 neither of the particles under consideration reached the steady-state equilibrium.

8. Conclusions

In our study, we found that the numerical simulation of aerosol with the help of a high size resolution continuous model (140 grid points for the particle size) reproduces quite realistically the observed features of the stratospheric Junge layer. The positive advective scheme with small diffusion (Smolarkiewicz and Grabowski 1989) worked equally well for advection and for condensation of both H_2SO_4 and H_2O. From the computational point of view, coagulation was the most time consuming among the processes, and if one attempts to perform the calculation in three dimensions, a more efficient strategy of calculation such as massively parallel processing must be sought. In summary, we think that the developed numerical scheme, especially after incorporating massively parallel processing, is easily applicable to various other problems involving aerosol and cloud drops.

Despite the somewhat arbitrary velocity profile and crude representation of dilution, our model possesses an excellent ability to represent certain realistic features of the stratospheric aerosol layer. The vertical profiles of the concentrations of particles of radii greater than or equal to 0.15 μm and 0.25 μm for the quiescent period resemble those measured by Hoffman and Rosen (1981) (autumn and winter 1978/79) and especially those by Junge et al. (1961) (autumn and winter 1959/60). Also, the vertical profiles of the concentration 1 yr after the eruption of Mt. Pinatubo resemble the profiles measured by Deshler et al. (1993). Additionally, for both periods, the decrease with altitude of the ratio of the

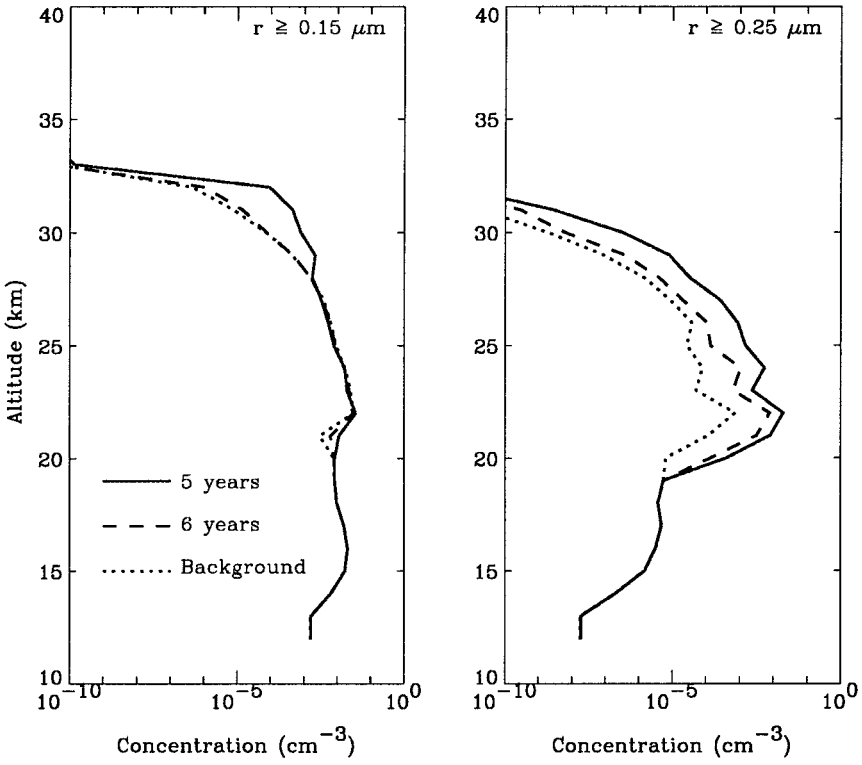

FIG. 10. Vertical profiles of the total number of particles of radii greater than or equal to 0.15 and 0.25 μm 5 yr and 6 yr after the eruption, and for the background state (scenario with OCS and CS_2).

concentration of particles of radii greater than or equal to 0.15 μm to that of radii greater than or equal to 0.25 μm is present. All these give us the confidence to draw certain conclusions and to formulate certain hypotheses of a general physical nature. Our numerical experiments indicate that, regardless of the selected velocity profile, the aerosol layer cannot be maintained without the injection of SO_2 during volcanic eruptions. The concentration of particles of radii greater than or equal to 0.15 and 0.25 μm obtained without volcanic source of SO_2 are too low. Even if certain uncertainties concerning the chemistry of such species like CS_2 or nucleation rates are removed, the temporal extent of the influence of the volcanic eruption on the aerosol layer is of the order of 5–6 yr. So we can safely say that the stratospheric aerosol layer is never a truly quiescent one, and that it exists as a quasi-stationary feature. Further, we have noticed that after the volcanic eruption, the concentration levels of large (submicron) particles remain elevated for long periods of time—up to six years. We also observed that the larger the particles the longer the influence of the volcanic eruption.

The results suggest that more insight into the physical processes of stratospheric aerosol can be obtained with more realistic eddy diffusion coefficients. If, instead of diffusion, advection due to the long-time-average velocity is used to mimic the motion in vertical, the results are very sensitive to the assumed vertical velocity profiles. This strongly indicates that dynamic processes are an important factor controlling the aerosol growth.

High resolution in size allows us to recognize various concentration modes both transient and quasi-stationary. For quiescent periods, two modes can be observed: the nucleation and growth modes; the former barely distinguishable if sufficiently high concentrations of H_2SO_4 are generated.

During volcanic periods, additional modes are present: due to nucleation on injected ash particles and due to condensational growth. The presence of both growth modes (background and volcanic) is well established in measurements (Deshler et al. 1993). We are also able to gain some insight into the character of the vertical profiles of the aerosol concentration. Two local maxima are observed. We attribute the generation of the lower maximum (20 km) to the condensational growth of both homogeneous liquid aerosol and aerosol with cores. We hypothesize that the observed second maximum of accumulation of particles (30 km) is based on the transition from the nucleation–condensation to the conversion–evaporation regime. Whether or not this mechanism plays an important role in the production of the aerosol remains to be examined with a three-dimensional version of the model.

REFERENCES

Andrews, D. G., J. R. Holton, and C. B. Leavy, 1987: *Middle Atmospheric Dynamics.* Academic Press, 498 pp.

Ayers, G. P., R. W. Gillett, and J. L. Gras, 1980: On the vapor pressure of sulfuric acid. *Geophys. Res. Lett.,* **7,** 433–436.

Brasseur, G. P., and S. Madronich, 1986: Chemistry-transport models. *Climate System Modelling,* K. E. Trenberth, Ed., Cambridge University Press, 491–518.

——, and S. Solomon, 1986: *Aeronomy of the Middle Atmosphere.* D. Reidel, 452 pp.

Brock, J. R., 1972: Condensational growth of atmospheric aerosols. *J. Colloid Interface Sci.,* **39,** 32–36.

Crutzen, P. J., 1976: The possible importance of CSO for the sulfate layer of the stratosphere. *Geophys. Res. Lett.,* **3,** 73–76.

DeMoore, W. B., and Coauthors, 1992: Chemical kinetics and photochemical data for use in stratospheric modeling. JPL Publication 92-20, Pasadena, CA, 185 pp.

Deshler, T., B. J. Johnson, and W. R. Rosier, 1993: Balloonborne measurements of Pinatubo aerosol during 1991 and 1992 at 41°N: Vertical profiles, size distribution, and volatility. *Geophys. Res. Lett.,* **20,** 1435–1438.

Fletcher, N. H., 1958: Size effect in heterogeneous nucleation. *J. Chem. Phys.,* **29,** 572–576.

Fuchs, N. A., 1964: *The Mechanics of Aerosols.* Pergamon Press, 398 pp.

——, and A. G. Sutugin, 1971: High dispersed aerosols. *Topics in Current Aerosol Research,* G. M. Hidy and J. R. Brock, Eds., Vol. 29, Pergamon Press, 572–576.

Gmitro, J. I., and T. Vermeulen, 1964: Vapor-liquid equilibria for aqueous sulfuric acid. *AIChE J.,* **10,** 740–746.

Hamill, P., C. S. Kiang, and R. D. Cadle, 1977a: The nucleation of H_2SO_4–H_2O solution aerosol particles in the stratosphere. *J. Atmos. Sci.,* **34,** 150–160.

——, O. B. Toon, and C. S. Kiang, 1977b: Microphysical processes affecting stratospheric aerosol. *J. Atmos. Sci.,* **34,** 1104–1119.

Haynes, P. H., C. J. Marks, M. E. McIntyre, T. G. Shepherd, and K. P. Shine, 1990: On the ''downward control'' of extratropical diabatic circulations by eddy-induced mean zonal forces. *J. Atmos. Sci.,* **48,** 651–678.

Hoffman, D. J., 1990: Increase in the stratospheric background sulfuric acid aerosol mass in the past 10 years. *Science,* **248,** 996–1000.

——, and J. M. Rosen, 1981: On the background stratospheric aerosol layer. *J. Atmos. Sci.,* **38,** 168–181.

——, and ——, 1984: On the temporal variation of stratospheric aerosol size and mass during the first 18 months following the 1982 eruption of El Chichón. *J. Geophys. Res.,* **89,** 4483–4890.

——, and S. J. Oltmans, 1992: The effect of stratospheric water vapor on the heterogeneous reaction rate of $ClONO_2$ and H_2O for sulfuric acid aerosol. *Geophys. Res. Lett.,* **19,** 2211–2214.

Jensen, E. J., O. B. Toon, H. B. Selkirk, J. D. Spinhirne, and M. R. Schoeberl, 1996: On the formation and persistence of subvisible cirrus clouds near the tropical tropopause. *J. Geophys. Res.,* **101,** 21 361–21 375.

Junge, C. E., C. W. Chagnon, and J. E. Manson, 1961: Stratospheric aerosols. *J. Meteor.,* **18,** 81–108.

Kasten, F., 1968: Falling speed of aerosol particles. *J. Meteor.,* **7,** 944–947.

Krueger, A. J., and R. A. Minzner, 1976: A mid-latitude ozone model for the 1976 U.S. Standard atmosphere. *J. Geophys. Res.,* **81,** 4477–4481.

Lilly, D. D., D. E. Waco, and S. I. Adelfang, 1974: Stratospheric mixing estimated from high-altitude turbulence measurements. *J. Appl. Meteor.,* **13,** 488–493.

Millikan, R. A., 1923a: Coefficients of slip in gases and the low of reflection of molecules from the surface of solids and liquids. *Phys. Rev.,* **21,** 217–238.

——, 1923b: The general low of fall of a small spherical body through a gas, and its bearing upon the nature of molecular reflection from surfaces. *Phys. Rev.,* **21,** 217–238.

Nair, P. V. N., and K. G. Vohra, 1975: Growth of aqueous sulphuric acid droplets as a function of relative humidity. *J. Aerosol Sci.,* **6,** 265–271.

Pitari, G., V. Rizi, L. Ricciardulli, and G. Visconti, 1993: High-speed civil transport impact: Role of sulphate, nitric acid trihydrate, and ice aerosols studied with a two-dimensional model including aerosol physics. *J. Geophys. Res.,* **98,** 23 141–23 164.

Pruppacher, H. R., and J. D. Klett, 1980: *Microphysics of Clouds and Precipitation.* D. Reidel, 714 pp.

Ramabhadran, T. E., T. W. Peterson, and J. H. Seinfeld, 1976: Dynamics of aerosol coagulation and condensation. *AIChE J.,* **22,** 840–851.

Roedel, W., 1979: Measurements of sulfuric acid saturation vapor pressure: Implications for aerosol formation by heteromolecular nucleation. *J. Aerosol Sci.,* **10,** 375–386.

Rosenlof, K. H., and J. R. Holton, 1993: Estimates of the stratospheric residual circulation using the downward control principle. *J. Geophys. Res.,* **98,** 10 465–10 479.

Sabinina, L., and L. Terpugov, 1935: Die Oberflächenspannung des Systems Schwefelsäure-Wasser. *Z. Phys. Chem.,* **A173,** 237–241.

Sheridan, P. J., R. C. Schnell, D. J. Hoffman, and T. Deshler, 1992: Electron microscope studies of Mt. Pinatubo aerosol layers over Laramie, Wyoming, during summer 1991. *Geophys. Res. Lett.,* **19,** 203–206.

Sissenwine, N., D. D. Grantham, and H. A. Salmela, 1968: Humidity up to the mesopause. *Air Force Surveys in Geophysics,* Vol. 206, 49 pp.

Smolarkiewicz, P. K., and W. W. Grabowski, 1989: The multidimensional positive definite advection transport algorithm: Nonoscilatory option. *J. Comput. Phys.,* **86,** 355–375.

Smoluchowski, M., 1917: Versuch einer mathematischen Theorie der Koagulationskinetik kolloider Lösungen. *Z. Phys. Chem.,* **92,** 9–168.

Steele, H. M., and P. Hamill, 1981: Effects of temperature and humidity on the growth and optical properties of sufphuric acid-water droplets in the stratosphere. *J. Aerosol Sci.,* **6,** 517–528.

Sze, N. D., and M. K. W. Ko, 1979: CS_2 and COS in the stratospheric sulphur budget. *Nature,* **280,** 308–310.

Tie, X., X. Lin, and G. Brasseur, 1994: Two-dimensional coupled dynamical/chemical/microphysical simulation of global distribution of El Chichón volcanic aerosol. *J. Geophys. Res.,* **99,** 16 779–16 792.

Toon, O. B., R. P. Turco, D. Westphal, R. Malone, and M. S. Liu, 1988: A multidimensional model for aerosols: Description of computational analogs. *J. Atmos. Sci.,* **45,** 2123–2143.

Turco, R. P., P. Hamill, O. B. Toon, R. C. Whitten, and C. S. Kiang, 1979: A one-dimensional model describing aerosol formation and evolution in the stratosphere: I. Physical processes and mathematical analogs. *J. Atmos. Sci.,* **36,** 699–717.

——, R. C. Whitten, and O. B. Toon, 1982: Stratospheric aerosols: Observation and theory. *Rev. Geophys. Space Phys.,* **20,** 233–279.

——, O. B. Toon, R. C. Whitten, P. Hamill, and R. G. Keesee, 1983: The 1980 eruption of Mount St. Helens: Physical and chemical processes in the stratospheric clouds. *J. Geophys. Res.,* **88,** 5299–5319.

Yue, G. K., and P. Hamill, 1979: The homogeneous nucleation rates of H_2SO_4-H_2O aerosol particles in air. *J. Aerosol. Sci.,* **10,** 609–614.

Zhao, J., R. P. Turco, and O. B. Toon, 1995: A model simulation of Pinatubo volcanic aerosols in the stratosphere. *J. Geophys. Res.,* **100,** 7315–7328.